Adsorption and Vibrational Spectroscopy of CO on Mordenite: Ab initio Density-Functional Study

T. Bučko,* J. Hafner, and L. Benco

Institut für Materialphysik and Center for Computational Material Science, Universität Wien, Sensengasse, A-1090 Wien, Austria

Received: January 10, 2005; In Final Form: February 8, 2005

We present a periodic density-functional investigation of the adsorption and the vibrational spectroscopy of CO in mordenite. Our results highlight a pronounced sensitivity of the strength of the hydrogen bond between the acidic hydroxyl groups and the adsorbed molecule, and hence of the induced red shift of the OH, and the blue shift of the CO stretching mode on the choice of the exchange-correlation functional. The popular Perdew−Wang (PW) gradient-corrected functional strongly overestimates the frequency shifts and the interaction energies. We demonstrate that the revised Perdew−Burke−Ernzerhof (RPBE) functional leads to an improved description of hydrogen bonding. For bridging OH groups, terminal silanol groups and for Lewis sites formed by tricoordinated Al atoms, we predict adsorption energies and frequency shifts in good agreement with experiment. The calculated difference in the binding energies of CO in purely siliceous mordenite and at Brønsted acid sites in the main channel agrees very well with microcalorimetry data. We find that Brønsted acid sites in the small channels (the side-pockets) of mordenite do not adsorb CO, which is adsorbed only in the main channel via the C atom. For these adsorption complexes we find reasonable (though not perfect) agreement of the predicted blue shift of the CO-mode and of the red shift of the OH-mode with experiment. Our prediction that the side-pockets are inaccessible to CO correlates well with the microcalorimetric studies and with experimental observation of the adsorption of O_2, N_2 and H_2 molecules but contradicts the current interpretation of experimental adsorption studies for CO.

I. Introduction

Although the chemical properties of bridged OH groups (Brønsted acid sites) and of terminal silanol groups in many zeolites have been studied extensively using various spectroscopies, the interpretation of the data remains controversial to some extent. For H-mordenite (and similarly for most other zeolites), the IR spectrum shows a weak adsorption band at 3747 cm^{-1} and a much stronger one centered at 3609 cm^{-1}.[1] It is generally agreed that the 3747 cm^{-1} band has to be attributed to OH stretching vibrations of terminal silanol groups centered at the outer surfaces.[1−3] The 3609 cm^{-1} band is assigned to the OH stretching modes of bridging hydroxyl groups, which constitute the main Brønsted acid sites of the zeolite. This band is somewhat asymmetric and may be deconvoluted into two components, a high-frequency (HF) mode centered at 3612 cm^{-1} and a low-frequency (LF) band centered at 3585 cm^{-1}.[1,4,5] The HF and LF bands were attributed to acidic hydroxyl groups in the main channels and in the small channels (side-pockets) of mordenite. A similar decomposition of the acidic OH stretching band into HF and LF components has also been reported for other zeolites, e.g., by Cairon et al.[6] and by Otero-Areán et al.[7] for Y-zeolite and by Bordiga et al.[8] for ferrierite. In the H−Y zeolite the HF and LF modes are attributed to hydroxyl groups in the supercage and inside the sodalite cages, respectively,[6,7] in ferrierite to acid sites in the large 10 MR rings and the 6 MR.[8] So far there seems to be general agreement. Upon dosing with small gas molecules (CO, O_2, N_2, H_2, ...), the HF component of the acidic OH band is quickly eroded away, whereas access to the sites generating the LF modes undergo smaller changes and are evidently not as easily accessible to probe molecules. Wakabayashi et al.[5,9] reported that the side-pockets of H-mordenite are inaccessible to N_2, O_2 and H_2 molecules, and Cairon et al.[6] concluded that CO adsorption leaves the LF component assigned to acid sites in the smaller sodalite cages of Y-zeolite unaffected. Bordiga et al.[8] reported that in H-ferrierite the acid sites in the 10 MR channels are more available to interaction with CO, N_2 and H_2, whereas sites in the small cages form weaker adducts. CO adsorption in H-mordenite has been studied by Webster et al.,[3] Bordiga et al.,[1] Maache et al.,[2] and Savitz et al.[10] Webster at al. performed a multiple equilibrium analysis MEA of the adsorption isoterms of a variety of adsorbates in Na- and H-mordenite. MEA can be used to identify the adsorption capacities and free energies for different processes: adsorption at Lewis sites, heterogeneous Brønsted sites and silanols. Interestingly, for O_2 adsorption only two processes (Lewis sites and BA sites at large channels) were identified, whereas four processes (including BA sites in the large and small channels) are required for N_2 and CO. In view of the smaller atomic diameter of O_2 compared to N_2 and CO it was concluded that only the higher polarizability of N_2 and CO enables an interaction with BA sites in the side-pockets. In contrast, the microcalorimetry studies of Savitz et al.[10] led to the conclusion that all BA sites accessible to CO are energetically equivalent. Bordiga et al. identified three peaks in the IR spectra of CO adsorbed in H-mordenite: an asymmetric main peak at 2172 cm^{-1} attributed to adsorption at BA sites, a weaker peak developing at high gas pressures assigned to CO physisorbed within the zeolite channels, and a very weak broad peak

* Corresponding author. E-mail: tomas.bucko@univie.ac.at.

10.1021/jp050151u CCC: $30.25
Published on Web 03/16/2005

attributed to adsorption at Lewis sites. Webster et al.[3] suggested that there is a linear relationship between the CO stretching frequencies and the process-specific free enthalpies of adsorption. Maache et al.[2] went one step further and deconvoluted the 2172 cm^{-1} peak into a 2177 cm^{-1} mode correlating with the LF OH modes and a 2168 cm^{-1} mode correlating with the HF OH modes. The assignment of the LF modes to BA sites in the small channels is supported by the fact that CO adsorption in the main channel (and hence at the HF sites) can be blocked by preadsorption of larger pyridine molecules. However, not all HF OH-groups can be blocked by pyridine adsorption and Maache et al. note that the LF OH groups are heterogeneous, some of them being strongly, others less acidic according to the red shift of the OH stretching modes.

Generally, it is assumed that CO adsorption at hydroxyl groups can occur only via the C atom. However, recently Otero-Areán et al.[7] argued that both OH···CO and OH···OC adducts are formed in a temperature-dependent equilibrium. For CO adsorbed in Y-zeolite, an enthalpy difference of 4.3 kJ/mol for the two different adsorption modes, favoring the C-adduct was reported. The assignment of the two components in the CO spectrum was based on the fact that CO adsorption leaves the LF component of the OH spectrum (assigned to BA sites in the small sodalite cages) totally unaffected so that an assignment to different types of BA sites seems to be excluded.

Besides the interaction with the acidic proton of Brønsted acid sites, the CO molecule interacts also with Lewis acid sites (LAS). Only little is known about the structure of LAS in zeolites and their role in the catalytic processes. Bolis et al.[11] associated Lewis acidity with coordinatively unsaturated Al^{3+} species. It has been found that at low coverages, the interaction of CO with Lewis sites dominates over interaction with BA sites. Adsorption enthalpies corresponding to the adsorption at LAS are 60−70 kJ/mol, depending on the zeolite type. In IR experiments, CO adsorbed at Lewis sites is characterized by bands above 2180 cm^{-1}.[5,12−15] Catana et al.[12] identified LAS by means of IR measurements. The IR bands assigned to CO adsorbed at LAS lie in a region between 2175 and 2208 cm^{-1}. It has been concluded that the extraframework Al particles constitute a significant fraction of strongest Lewis acid sites ($\Delta\nu_{CO} > 43$ cm^{-1}). It should be noted that the possibility of occurrence of LAS that are weaker in terms of acidity and interaction energy than BA sites has been overlooked.

Although the adsorption of CO at various sites of zeolites has been frequently studied theoretically, the investigations have been performed using either cluster ab initio[16−21] or embedded cluster techniques.[11,22−24] Especially the former approach is limited by the small number of atoms used to model active site. Moreover, the nonspecific interactions of the adsorbate with the zeolite framework are completely neglected. In the present study we employ periodic ab initio DFT techniques to investigate adsorption complexes of CO at different active sites in mordenite. In addition to surface terminal silanol groups and Brønsted acid sites in the main channel and in the side-pockets, structural defects representing Lewis sites of different strength are investigated.

II. DFT Methodology

A. Exchange-Correlation Functionals and Hydrogen Bonding. Periodic ab initio DFT calculations have been performed using the VASP code.[25−28] Initially, for the exchange-correlation functional the generalized gradient approximation (GGA) of Perdew and Wang (PW91)[29,30] has been used. The PW91 functional is known to provide an excellent description of the binding energy, the geometry and the vibrational properties of a wide range of molecules and solids, including zeolites.[31−33] This functional has also been used extensively to explore the potential energy surfaces for the adsorption of small molecules at metallic oxides.[34] Generally, excellent agreement of the calculated adsorption geometry and of the vibrational spectra of the adsorption complexes has been achieved,[34] although a tendency to overestimate the adsorption energy is evident. It has been shown that this overestimation can be corrected by adopting the exchange-correlation functional proposed by Perdew, Burke, and Ernzerhof[35] as modified by Hammer, Hansen and Norskov[36]—hereafter this functional is referred to as RPBE. In the present study we have found that calculations using the PW91 exchange-correlation functional tend to overestimate the strength of the hydrogen bond mediating the adsorption of a weakly basic molecule such as CO at Brønsted acid sites and at silanol groups. The same conclusion holds for the original version of the PBE functional, whereas the revised RPBE functional leads to more realistic results. The conclusion that the RPBE functional provides a more realistic description of a hydrogen-bonded system has general validity. This was demonstrated by the investigations of hydrogen-bonded dimers of water and methanol: although calculations using the PBE and PW91 functionals overestimate the red shift of the OH stretching frequencies induced by the dimerization, the RPBE functional leads to good agreement with calculations using hybrid functionals including a fraction of exact exchange of using higher level SCF approaches. Details of these studies will be published elsewhere. In the present paper results obtained using both the PW91 and the RPBE functionals will be presented.

B. DFT Calculations for Large Systems. The Kohn−Sham equations have been solved variationally on a plane-wave basis set using the projector-augmented-wave (PAW) method of Blöchl,[37] as recently adapted by Kresse and Joubert.[38] The Brillouin-zone sampling was restricted to the Γ-point, the plane-wave cutoff was set to 400 eV. The convergence criterion for the electronic self-consistency cycle is that the change in the total energy is smaller than 10^{-5} eV/atom between successive steps. All atomic positions have been relaxed using a conjugate gradient algorithm.

The lattice parameters for bulk mordenite have been fixed to the values optimized recently by Demuth et al.[31] ($a = b = 13.655$ Å, $c = 7.606$ Å) using the PW91 functional. Calculations using the PBE and RPBE lead only to small differences in the lattice parameters and internal coordinates ($\Delta a = \Delta b = \sim 0.09$ Å, $\Delta c = \sim 0.05$ Å). Note that the primitive monoclinic instead of the conventional orthorhombic unit cell has been used (see Figure 1). In the slab models used to investigate the surface, the lattice vector perpendicular to the surface plane was elongated in such a way that the repeated layers were separated by a vacuum region of 8 Å. The lattice vectors *a* and *b* are the same as for the bulk model, $a = b = 13.655$ Å, $c = 18.500$ Å. The thickness of the slab is ∼10.5 Å.

The slab model of the (001) surface of mordenite is created from the bulk structure by cutting through the bridging oxygen atoms along (001) plane. Equivalent surfaces are present on both sides of the slab. Under-coordinated surface Si atoms have been terminated with OH groups. Out of two possible cleavage planes (see ref 39) we have chosen the one cutting through the center of largest pore. An alternative cleavage plane would require by about 50% more atoms in unit. Details on the modelization of the (001) surface of mordenite can be found in our recent paper.[39]

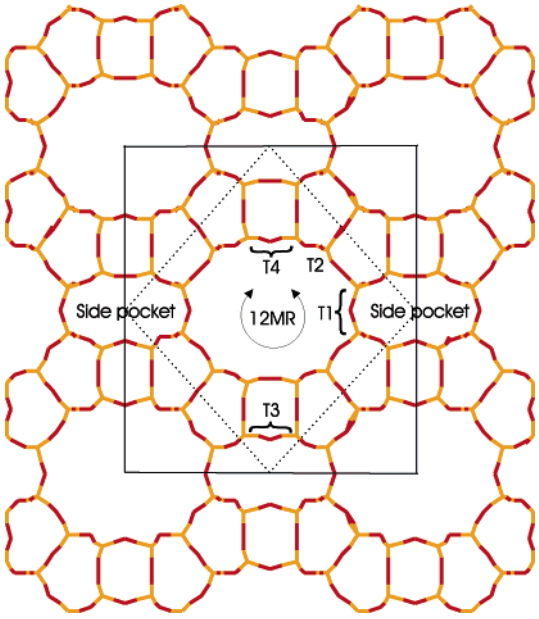

Figure 1. Conventional orthorhombic cell (solid frame) and the primitive monoclinic cell used in this work (dashed frame). Positions of symmetrically nonequivalent tetrahedral sites (T1−T4), main channel (12MR) and small channel are shown.

C. Theoretical Vibrational Spectroscopy. The harmonic vibrational frequencies are calculated numerically using a finite difference method. The elements of the second derivatives (Hesse) matrix are calculated using the formula

$$H_{i,j} = \frac{\partial^2 E}{\partial x_i \partial x_j} = \frac{g(x_j)^+ - g(x_j)^-}{2\Delta x_i} \quad (1)$$

where $g(x_j)^+$ ($g(x_j)^-$) is the force in the direction of the coordinate x_j induced by a small positive (negative) displacement of Cartesian coordinate Δx_i. Forces $g(x_j)$ are calculated analytically. In our calculations, a value of 0.02 Å has been used for Δx_i. The harmonic vibrational frequencies are given by

$$\nu_{e,i} = \sqrt{\frac{\lambda_i}{4\pi^2 c^2}} \quad (2)$$

where λ_i is an eigenvalue of the mass-weighted Hesse (dynamical) matrix **D**

$$\mathbf{D} = \mathbf{M}^{-1}\mathbf{H}\mathbf{M}^{-1} \quad (3)$$

The calculation of the full dynamical matrix for large systems is a computationally demanding task. On the other hand vibrational modes of molecules adsorbed at the substrate are expected to be affected only by the nearest atoms of the substrate. It is also well-known that the OH stretching modes of the acid sites are almost pure eigenmodes and separated from the vibrational modes of the framework atoms.[40] According to our experience on the characterization of a BA site, the dynamical matrix calculated for a complex consisting of the adsorbed molecule, the OH group and only two neighboring tetrahedral sites (i.e., Al and Si atoms) gives essentially identical results for the OH stretching frequencies and the vibrational modes of the adsorbate to those derived from the full dynamical matrix for all atoms in the supercell.[41] Therefore, only results calculated using partial dynamical matrixes are presented.

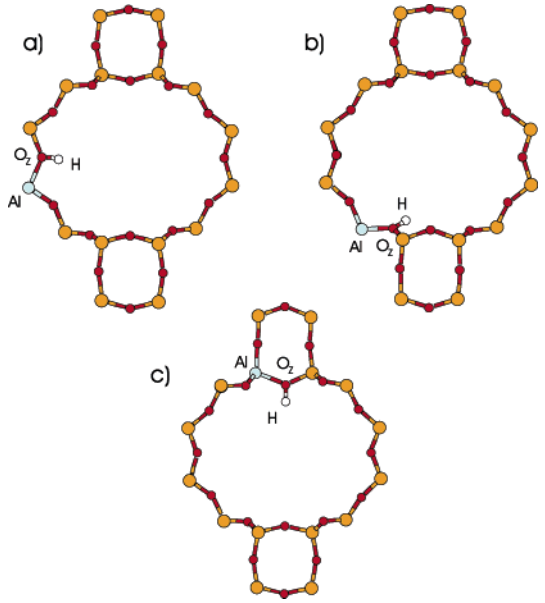

Figure 2. Brønsted acid sites located in the main channel of mordenite: Al1−O7 (a), Al2−O2 (b) and Al4−O10 (c).

III. Structural Models for Active Sites

In present study we modelize the following Brønsted sites:

•Brønsted acid (BA) sites in the main channel of mordenite: Al1−O7, Al2−O2 and Al4−O10 (see Figure 2). Their average OH stretching frequencies are 3717 cm^{-1} (PW91) and 3712 cm^{-1} (RPBE).

•BA sites in the small channel of mordenite: Al3−O9, Al3−O6 and Al1−O6 (see Figure 3). The average OH stretching frequencies are 3693 cm^{-1} (PW91) and 3704 cm^{-1} (RPBE). For the characterization of the BA sites we refer to the work of Demuth et al.[31] The notation for tetrahedral and oxygen sites is as in Schlenker et al.[42]

•Terminal silanol groups at the (001) surface of mordenite TSil1 and TSil2 (see Figure 4) (for details on modelization of the (001) surface of mordenite see Ref. 39). Average OH stretching frequencies are 3809 and 3798 cm^{-1} (RPBE).

The calculated OH bond lengths and the harmonic OH stretching frequencies (ν_{eOH}) for unperturbed sites used as references throughout this study are collected in Table 1. The differences between values calculated using PW91 and RPBE functionals are rather modest and without any obvious trend. In agreement with experiment, the OH stretching frequencies for terminal silanol groups are upshifted by about 100 cm^{-1} compared to those for BA sites. The OH stretching frequencies of BA sites in the main channel calculated using PW91 functional are by 23 cm^{-1} higher than those of BA sites in the small channel (see Table 1). Although this result agrees with experiment, it should be noted that a certain overlap between these two types of BA sites is expected (e.g., ν_{eOH} for Al1−O7 is even lower than that for Al1−O6). The overlap is even larger in RPBE calculations, the average OH stretching frequencies of the BA sites in the main channel and in the side-pockets are almost identical, the difference being only 8 cm^{-1}.

Structural defects at the (001) surface of mordenite created by dehydration have been shown to be formed at relatively mild conditions.[43] In this study we consider those defects which are favorable on the basis of energetics: (i) a two-membered silica ring (2MR) (see Figure 5a), (ii) a two-membered silica ring with a BA site (2MR−Al) (see Figure 5b) and a defect with a 3-fold coordinated Al atom (3-Al) (see Figure 5c). The 2MR and 3-Al defects represent aprotic (i.e., Lewis) sites whereas the

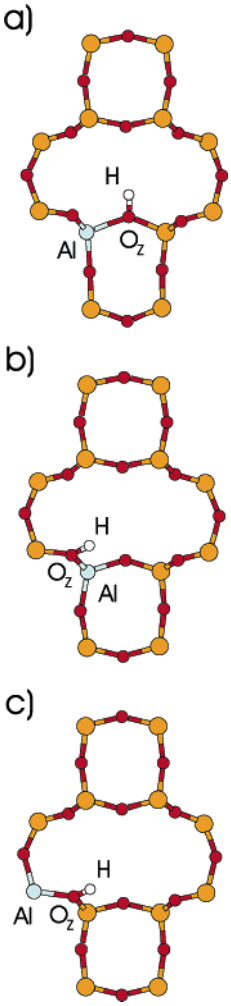

Figure 3. Brønsted acid sites located in the small channel of mordenite: Al3−O9 (a), Al3−O6 (b) and Al1−O6 (c).

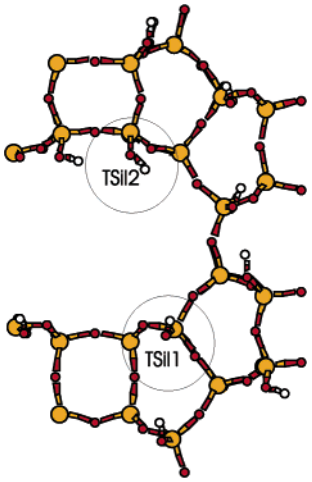

Figure 4. Top view of the (001) surface of mordenite. Terminal silanol groups TSil1 and TSil2 investigated in this study are marked by circles.

2MR−Al defect comprises both a weak Brønsted site and a Lewis center (Al site). The OH stretching frequency for defect 2MR−Al of 3780 (3773) cm^{-1} calculated using PW91 (RPBE) functionals (see Table 1) indicates rather low acidity of the site.

IV. CO in Vacuum and in the Zeolite

The only vibrational eigenstate of the CO molecule is the CO stretching vibration (ν_{CO}) at 2143 cm^{-1};[44] the length of the C═O bond is 1.128 Å.[45] The calculated CO bond length of a free CO molecule is 1.143 Å (PW91) and 1.149 Å (RPBE), respectively, and the harmonic CO stretching frequency is 2131 cm^{-1} (PW91) and 2118 cm^{-1} (RPBE). The interatomic distance calculated using both functionals is thus longer and the corresponding stretching frequency is lower than experimental data, the PW91 functional leads to slightly better agreement with experiment. When located in the main channel of pure siliceous mordenite (see Figure 6a), the CO molecule interacts only weakly with framework atoms, calculated binding energies being 4.2 kJ/mol (PW91) and 5.9 (RPBE). In the relaxed structure, the CO is located in the middle of the channel, the distance between CO and the nearest atom of framework is ∼3.50 Å. The CO bond length is unchanged and ν_{eCO} is changed negligibly compared to gas-phase CO (upshifted by 3 cm^{-1} with PW91 and downshifted by 2 cm^{-1} using RPBE functional, respectively).

In Figure 6b, CO adsorbed in the small channel is shown. Due to the confinement effect, CO gets closer to framework atoms. The interaction energy calculated using PW91 functional is slightly higher compared to CO in the main channel (ΔE_{ads} = 7.4 kJ/mol). The CO bond is elongated by only 0.001 Å and

TABLE 1: Lengths of OH Bonds and Harmonic OH Stretching Frequencies ν_{eOH} for Brønsted Acid Sites in the Main Channel (Al1−O7, Al2−O2 and Al4−O10), Brønsted Acid Sites Located in the Small Channel (Al3−O9, Al3−O6 and Al1−O6), and Unperturbed Terminal Silanol Groups (TSil1 and TSil2) and for a Surface Defect with a BA Site at the Two-Membered Ring (2MR−Al) (cf. Figures 2−5)[a]

	OH (Å)	ν_{eOH} (cm^{-1})
Al1−O7	0.977 (0.977)	3703 (3703)
Al2−O2	0.975 (0.974)	3728 (3742)
Al4−O10	0.976 (0.977)	3717 (3691)
Al3−O9	0.980 (0.978)	3687 (3694)
Al3−O6	0.978 (0.977)	3688 (3703)
Al1−O6	0.976 (0.976)	3705 (3715)
TSil1	0.969 (0.971)	3798 (3788)
TSil2	0.968 (0.970)	3820 (3807)
2MR−Al	0.971 (0.972)	3780 (3773)

[a] Results obtained using both the PW91 and RPBE (in parentheses) are listed.

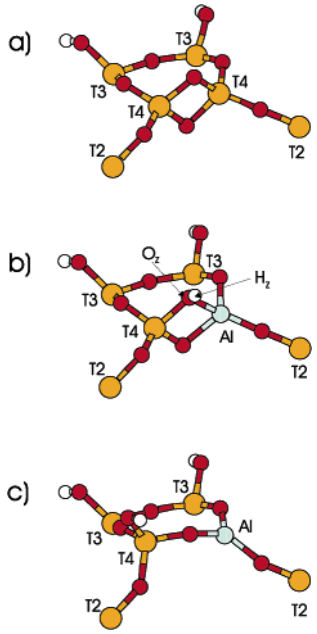

Figure 5. Detailed view of defect with two-membered silica ring (a), defect with BA site at two membered ring (b), and 3-fold coordinated surface Al site (c).

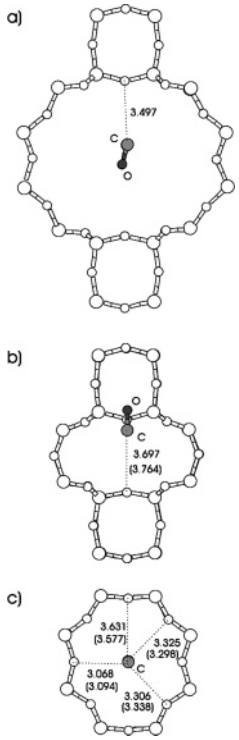

Figure 6. Carbon monoxide adsorbed in the main channel (a) and in the small channel ((b) top view, (c) side view) of purely siliceous mordenite. Distances between CO and nearest framework atoms are given in Å as calculated using the PW91 functional (RPBE values are given in parentheses).

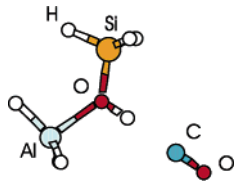

Figure 7. Cluster model of Brønsted acid side interacting with carbon monoxide.

the CO stretching frequency is red-shifted by 7 cm^{-1}. The RPBE functional provides completely different results: the adsorption in the side channel is endothermic ($\Delta E_{ads} = -9.1$ kJ/mol) and the CO stretching frequency red-shifted by 14 cm^{-1}. The change in the CO bond length is 0.001 Å.

V. Brønsted Acid Sites

A. Models for Brønsted Acid Sites. A number of theoretical investigations of adsorption of carbon monoxide at BA sites of a zeolite have been performed using a cluster approach.[16,17,21] To investigate the influence of size of the model on the quality of results, we have tested following models for site Al4−O10 (see Figure 2c):

A dimer cluster contains only two tetrahedral units (Si and Al atoms), which are connected via the protonated oxygen atom (O_Z), see Figure 7. Three dangling bonds per tetrahedral atom are terminated by H atoms. This model has been widely used in recent theoretical investigations.[16,17]

A model with one-dimensional periodicity (chain model); see Figure 8. Every tetrahedral site is connected to two neighboring tetrahedral sites via O atoms, two dangling bonds per tetrahedral atom are terminated by H atoms.

A model with two-dimensional periodicity (thin 2D-framework); see Figures 9 and 10. Every tetrahedral site is connected to three neighboring tetrahedral atoms via O atoms; one terminal H atom is used per tetrahedral site.

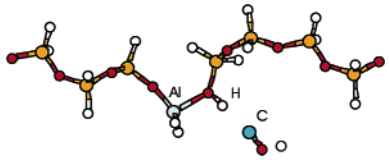

Figure 8. Chain model of Brønsted acid side interacting with carbon monoxide.

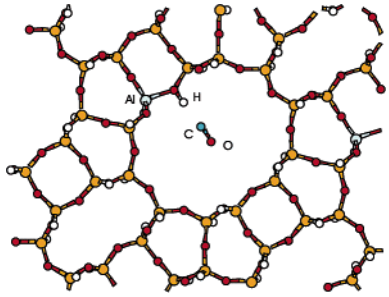

Figure 9. Top view of 2D-framework model of mordenite with Brønsted acid interacting with CO.

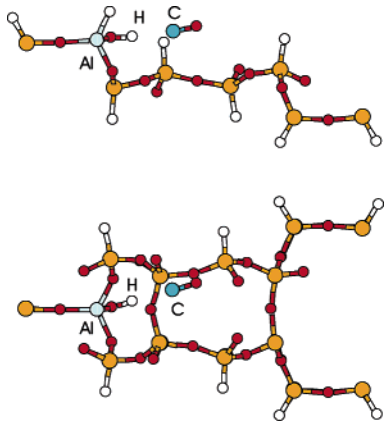

Figure 10. Side view of models with two-dimensional periodicity of mordenite with Brønsted acid interacting with CO: thin 2D-framework model (above) and slab model (below).

A model with two-dimensional periodicity (slab model) (Figures 9 and 10) contains tetrahedral sites with four bridged O atoms and sites with three bridged O atoms and with one terminal H atom. This model (but terminated by OH groups instead of H atoms) is used for the modelization of the (001) surface of mordenite.[39]

A periodic model of the bulk structure of acidic mordenite (see Figures 2). This model contains only $T-O_4$ units.

The initial geometry is taken from the relaxed periodic model of bulk mordenite with Al substituted in the position Al4−O10 (see Figure 2). Although the natural termination of unsaturated tetrahedral sites at external surfaces of zeolites is that by hydroxyl groups,[39,46] due to problems caused by the strong dipole moment of OH groups and with artificial H-bonding between OH groups yielding unrealistic geometries, a termination by H atoms is usually used in cluster calculations.[16] For these reasons, H-termination is used also in our tests. We stress that a termination by OH groups is necessary for a realistic modelization of external surfaces of zeolites.[39] The cell parameters are scaled in such a way that distances between atoms of two consecutive layers are at least 5 Å.

Geometries of the BA sites and the OH stretching frequencies calculated using the PW91 and RPBE functionals for different

TABLE 2: Selected Structural Parameters and Harmonic OH Stretching Frequencies for Different Models of the BA Site Al4−O10 (cf. Figures 2 and 7−10) Calculated Using the PW91 and RPBE (in Parentheses) Functionals

model (Å)	Al−O_Z (Å)	Si−O_Z (deg)	AlO_ZSi (Å)	O_Z-H (cm^{-1})	ν_{eOH}
cluster	2.025	1.708	132.8	0.973	3744
	(2.057)	(1.723)	(125.8)	(0.973)	(3746)
chain	2.003	1.710	135.4	0.975	3698
	(2.034)	(1.717)	(137.7)	(0.975)	(3704)
2D-framework	1.949	1.710	137.8	0.977	3684
	(1.988)	(1.721)	(137.5)	(0.978)	(3688)
slab	1.885	1.695	136.3	0.977	3696
	(1.900)	(1.704)	(135.1)	(0.976)	(3711)
bulk	1.874	1.683	134.0	0.976	3717
	(1.893)	(1.701)	(133.2)	(0.977)	(3691)

structural models are collected in Table 2. In this section we discuss only the PW91 results in detail. However, qualitatively very similar conclusions can be made on the basis of RPBE calculations. The bond length Al−O_Z decreases monotonically with growing size of the model (2.025 Å for cluster, 1.874 Å for the bulk model). The calculated Si−O_Z bond lengths are almost same for cluster, chain and 2D-framework models (1.708−1.710 Å), respectively, but differ significantly from those for models in which Al and Si atoms of BA site are not terminated with H atoms, i.e., the slab and bulk models (1.695 and 1.683 Å, respectively). The AlO_ZSi angle changes only moderately with increasing size of the model, the difference between the cluster model and the bulk being only 1.2°. The bond length O_Z−H calculated for the cluster model (0.973) differs by −0.003 compared to bulk result. The O_Z−H bond lengths for other models differ only by ±0.001 Å from the bulk. The calculated harmonic OH stretching frequency in the bulk is 3717 cm^{-1}. The harmonic OH stretching frequency for the cluster model is higher by 27 cm^{-1}.

In Table 3 the calculated binding energies, CO and OH stretching frequencies and geometries of adsorption complexes at a Brønsted acid site as calculated for different models are collected. The calculated binding energies vary with respect to the model size, the difference between bulk model and the minimal cluster is as large as 7.9 kJ/mol. It should be emphasized that except for slab and bulk models, an error of about 4 kJ/mol is introduced by neglecting the long-range interactions of CO with the framework atoms (see previous section).

The structural parameters such as the OH, Al−O_Z, and Si−O_Z bond lengths show obvious trends with respect to the model size (see Table 3). Compared to the bulk, the harmonic OH stretching frequencies for other models are increased (the OH stretching frequency correlates with the O_Z−H bond length) due to a strong reduction of the red shift induced by the CO adsorption. The smaller red shift correlates with lower adsorption energy calculated using the cluster models. Thus the harmonic OH stretching frequency calculated for the cluster model is higher by 150 cm^{-1} compared to the bulk. The combined error in the shift of the harmonic OH stretching frequency introduced by an incorrect geometry and by the artificial termination of the tetrahedral atoms is therefore 123 cm^{-1}.

The C═O bond length is almost constant for all models (1.137−1.138 Å). Also difference in shift of harmonic CO stretching frequency varies only between −7 and +4 cm^{-1} compared to that for bulk model.

By direct comparison of the results obtained with the simple dimer cluster with the bulk results, we conclude that the former not only does not allow us to distinguish between BA sites at different crystallographic positions but also provides an incorrect description of the geometry, the interaction energy and the vibrational properties of the adsorption complex of CO with a BA site. The chain and 2D-framework models provide only minor improvements over the minimal cluster model. Obviously, the main reasons are completely artificial termination of tetrahedral atoms near the bridging OH group by H atoms in these three models and the absence of natural geometrical restrictions due to the periodic crystal structure.

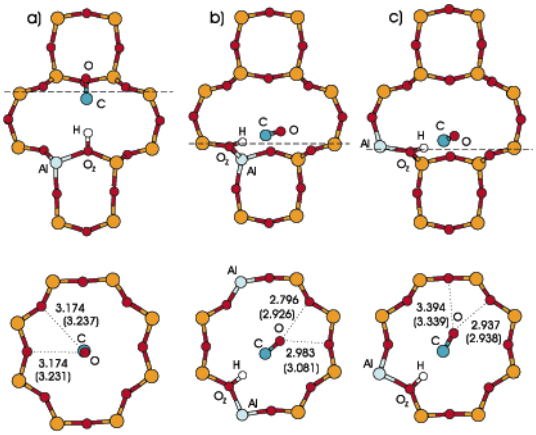

Figure 11. (Above) top view of carbon monoxide adsorbed at sites Al3−O9 (a), Al3−O6 (b), and Al1−O6 (c) located in small channel. The eight-membered ring closest to the CO molecule is marked by a dashed line (above) and displayed in detail (below). Distances between the oxygen atom of the CO molecule and O atoms in the 8 MR are given in Å, as calculated using the PW91 functional, with RPBE values in parentheses.

B. Geometry and Energetics. At low coverages, the carbon monoxide molecule forms weakly hydrogen bonded 1:1 complexes with bridged OH groups.[10] On the basis of the experimental and theoretical investigations[16,17,47] it follows that CO interacts with the OH group predominantly via its C end. For the sake of completness, however, we report also results for adsorption via the O end of CO.

Selected structural parameters for the adsorption complexes of CO at three different BA sites in the main channel (i.e., Al1−O7, Al2−O2 and Al4−O10) calculated using both the PW91 and the RPBE functionals are given in Table 4. The separations between the CO molecule and the H atom of the BA sites are 1.896 (2.069) Å, 1.906 (2.049) Å, and 1.926 (2.015) Å for Al1−O7, Al2−O2 and Al4−O10, respectively. The pronounced elongation of the length of the hydrogen bond (Cx distance, see Table 4) on replacing the PW91 by the RPBE functional varying between 0.17 Å (Al1−O7) and 0.09 Å (Al4−O10) correlates with a strong reduction of the binding energy (varying between 10.7 kJ/mol (Al1−O7) and 17.5 kJ/mol (Al2−O2)). The lengths of CO bonds are 1.137 (1.144) Å using the PW91 (RPBE) functionals, i.e., shortened by 0.006 (0.005) Å compared to the free CO molecule in all complexes; the O_Z−H distances are about 1.000 (0.992) Å (i.e., on average elongated by about 0.024 (0.016) Å compared to the O_Z−H lengths of unperturbed BA sites).

Carbon monoxide adsorbed at BA sites in the small channel (i.e., Al3−O9, Al3−O6 and Al1−O6) is shown in Figure 11. The CO bonding to Al3−O9 is positioned in such a way that it points into the center of 8MR (see Figure 11a), distances between the CO molecule and atoms in the 8MR being larger than 3.1 Å. In adsorption at the BA sites Al3−O6 and Al1−O6, CO interacts more strongly with framework atoms due to the location of the OH groups of BA sites. Separations between the O atom of CO and O atoms of the framework are smaller than 3 Å (see Figure 11b,c). Evidently, the geometry of the

TABLE 3: Binding Energies, Selected Structural Parameters and Harmonic OH Stretching Frequencies for Different Models of the BA Site Al4−O10 Interacting with CO (cf. Figures 7−10) Calculated Using the PW91 and RPBE (in Parentheses) Functionals

model	ΔE_{ads} (kJ/mol)	Al−O_Z (Å)	Si−O_Z (Å)	AlO_ZSi (deg)	O_Z−H (Å)	C═O (Å)	C···H (Å)	ν_{eOH} (cm^{-1})	ν_{eCO} (cm^{-1})
cluster	16.5	1.996	1.697	134.1	0.990	1.137	1.951	3366	2183
	(5.9)	(2.042)	(1.714)	(133.7)	(0.984)	(1.145)	(2.131)	(3497)	(2160)
chain	13.3	1.986	1.700	135.7	0.991	1.138	1.980	3360	2173
	(1.2)	(2.032)	(1.712)	(135.8)	(0.985)	(1.145)	(2.126)	(3482)	(2157)
2D-	17.6	1.932	1.695	138.4	0.996	1.137	1.941	3281	2177
-framework	(4.8)	(1.957)	(1.708)	(138.3)	(0.990)	(1.144)	(2.032)	(3379)	(2165)
slab	17.8	1.871	1.679	135.2	0.999	1.137	1.934	3219	2172
	(8.3)	(1.889)	(1.691)	(134.4)	(0.992)	(1.144)	(2.039)	(3355)	(2165)
bulk	24.4	1.860	1.674	134.6	1.000	1.137	1.926	3216	2179
	(11.5)	(1.877)	(1.688)	(133.7)	(0.993)	(1.144)	(2.015)	(3337)	(2165)

TABLE 4: Binding Energies, Selected Structural Parameters and CO and OH Stretching Frequencies Calculated for CO Interacting with Active Sites via the C Atom, Using the PW91 and RPBE (in Parentheses) Functionals

	ΔE_{ads} (kJ/mol)	Cx (Å)	O_ZH (Å)	ν_{eCO} (cm^{-1})	ν_{eOH} (cm^{-1})
Al1−O7	22.2	1.896	1.001	2174	3182
	(11.5)	(2.069)	(0.992)	(2159)	(3374)
Al2−O2	26.1	1.906	1.000	2178	3205
	(8.6)	2.049)	(0.991)	(2154)	(3366)
Al4−O10	24.4	1.926	1.000	2179	3216
	(7.0)	(2.015)	(0.993)	(2165)	(3337)
Al3−O9	18.9	1.859	1.008	2179	3070
	(−6.8)	(1.977)	(0.999)	(2165)	(3228)
Al3−O6	7.9	1.773	1.012	2199	2991
	(−16.0)	(1.802)	(1.006)	(2197)	(3068)
Al1−O6	12.8	1.791	1.001	2186	3025
	(−12.9)	(1.813)	(1.005)	(2185)	(3088)
TSil1	8.9	2.134	0.978	2155	3620
	(2.4)	(2.312)	(0.975)	(2134)	(3689)
TSil2	10.3	2.149	0.977	2157	3629
	(2.0)	(2.256)	(0.974)	(2146)	(3700)
2MR−Al	15.4	1.989	0.985	2169	3458
	(8.3)	(2.105)	(0.981)	(2158)	(3542)
3-Al	52.1	2.173	-	2193	
	(32.6)	(2.230)	-	(2183)	

[a] Cx stands for the distance between C and H for proton-containing sites and for the distance between C and Al for defect 3-Al. For notation, see Figures 2−5.

TABLE 5: Binding Energies, Selected Structural Parameters and CO and OH Stretching Frequencies Calculated Using the PW91 and RPBE (in Parentheses) Functionals for CO Interacting with Active Sites via O Atom

	ΔE_{ads} (kJ/mol)	Ox (Å)	O_ZH (Å)	ν_{eCO} (cm^{-1})	ν_{eOH} (cm^{-1})
Al1−O7	8.8	1.959	0.983	2108	3572
	(2.2)	(2.174)	(0.979)	(2101)	(3656)
Al2−O2	12.6	1.954	0.981	2105	3590
	(0.7)	(2.185)	(0.977)	(2093)	(3671)
Al4−O10	11.7	1.952	0.983	2106	3569
	(2.7)	(2.240)	(0.978)	(2100)	(3667)
Al3−O9	1.4	1.819	0.987	2107	3490
	(−20.6)	(1.973)	(0.982)	(2121)	(3588)
Al3−O6	−7.7	1.776	0.986	2097	3485
	(−31.4)	(1.859)	(0.982)	(2093)	(3567)
Al1−O6	−10.6	1.793	0.985	2103	3507
	(−29.3)	(1.891)	(0.982)	(2093)	(3570)
TSil1	2.7	2.198	0.971	2115	3780
	(−1.2)	(2.411)	(0.970)	(2115)	(3812)
TSil2	3.4	2.114	0.971	2113	3776
	(−1.8)	(2.282)	(0.970)	(2106)	(3812)
2MR−Al	5.5	1.992	0.974	2110	3706
	(1.3)	(2.159)	(0.973)	(2103)	(3746)
3-Al	16.9	2.200	-	2094	-
	(2.1)	(2.328)	-	(2085)	-

[a] Ox stands for the distance between C and H for proton-containing sites and for the distance between O and Al for defect 3-Al. For notation, see Figures 2−5.

adsorption complexes is affected by the more constrained environment: on average, the PW91 (RPBE) calculations produce distances between the C atom and the H atom of the BA sites shortened by about 0.102 (0.180) Å, and the O_ZH distances are on average by 0.007 (0.011) Å longer compared to those of BA sites in the main channel. The CO bond lengths are 1.136 (1.144) Å, 1.134 (1.140) Å and 1.135 (1.141) Å for models Al3−O9, Al3−O6 and Al1−O6, respectively, i.e., slightly shorter than those of CO adsorbed at the BA sites in the main channel.

The average binding energy for the adsorption at the BA sites in the main channel is 24.2 kJ/mol using PW91 and 9.0 kJ/mol using the RPBE functionals (see Table 4). The adsorption in the side channel is, due to the additional repulsive interaction with framework O atoms, energetically less favorable compared to the adsorption in the main channel. Though the difference in the binding energies is relatively modest in calculations based on the PW91 functional (average binding energy is ∼13.2 kJ/mol), the RPBE calculations predict a massive reduction of the adsorption strength—the binding energies are even negative (average $\Delta E_{ads} = -11.9$ kJ/mol). A possible adsorption of CO in the small channels would hence be stabilized by van der Waals forces only. We also note that although for BA sites in the main channel the change of the DFT functional also affects the energetic order of the sites, this is not the case for the BA sites in the small channels. This indicates that the energetic order is largely determined by the repulsive interactions. Theoretical binding energies can be compared with the heat of adsorption of CO in purely siliceous and H-mordenite measured by Savitz et al.[10] From microcalorimetric measurements it was concluded that the isosteric heats of adsorption are about 17 kJ/mol in purely siliceous samples and 26.5 kJ/mol in H-mordenite. The adsorption energy in the purely siliceous material is essentially independent of coverage, in H-mordenite the heat of adsorption falls to ∼17 kJ/mol once the number of adsorbed CO molecules exceeds the concentration of Brønsted sites estimated from TPD measurements with isopropylamin. Savitz et al. emphasize that their results are consistent with all of the Brønsted acid sites being energetically equivalent. Combined with the fact that only BA sites in the main channel are accessible to the large probe molecules in their TPD experiments, we take this as indirect evidence that CO is adsorbed in the main channel only.

The adsorption energies and structural data for CO molecules adsorbed at BA sites via the O atom are reported in Table 5. The difference between BA sites in the main channel and those in the side-pocket is even more significant. The binding energy calculated using PW91 (RPBE) varies between 8.8 (0.7) kJ/mol and 12.6 (2.7) kJ/mol for BA sites in the main channel, and between −10.6 kJ/mol (−31.4) and 1.4 (−20.6) kJ/mol for

those in the small channel. Hence according to the RPBE calculations, adsorption via the O atom is excluded in the side-pockets (even considering a stabilizing contribution from the vdW forces), and extremely weak in the main channel. For BA sites in the main channel, average separations between the CO molecule and the H atom of the BA site are larger by 0.042 (0.155) Å compared to those for C-adducts in the main channel. For O-adducts in the small channel the distance between carbon monoxide and the H atom differs much less from the C-adducts. This is mainly an effect of the repulsive interaction with framework atoms in the confined space of the small channel. Although the CO bond lengths are very similar for all O-adducts (1.144−1.145 Å in PW91, 1.148−1.151 Å in RPBE), the lengths of the hydroxyl bonds in O-adducts at BA sites in the main channel are on average 0.003 (0.004) Å longer compared to those in the main channel. Compared to those of C-adducts, the O_ZH bonds in O-adducts are significantly shorter; this is ascribed to much weaker interaction with the BA site.

Evidently, calculations using the PW91 and RPBE functionals lead to significant differences in the predicted adsorption behavior of CO in H-mordenite. PW91 calculations yield average binding energies of 24.2 kJ/mol for C-on adsorption in the main channel and 13.9 kJ/mol in the side-pockets, and still 11.0 kJ/mol for O-on adsorption in the main channel. RPBE calculations predict the side-pockets to be virtually inaccessible to CO, whereas in the main channel both OH···CO and OH···OC hydrogen bonded species can exist in a temperature-dependent equilibrium, average binding energies being 9.0 kJ/mol for the C-adduct and 1.9 kJ/mol for the O-adduct. The average difference in the binding energy of 7.1 kJ/mol can be compared with the experimental estimate of 4.3 kJ/mol measured for CO adsorbed at zeolite H−Y.[7]

C. Vibrational Properties. The IR spectra of CO adsorbed at BA sites in mordenite have been measured by Maache et al.[2] It has been claimed that the CO stretching frequency is blue-shifted by 34 cm^{-1} upon adsorption in the main channel (i.e., at BA sites responsible for high-frequency modes), and by 26 cm^{-1} upon adsorption in small channel (i.e., at low-frequency BA sites). Corresponding shifts of OH stretching frequencies are −260 and −332 cm^{-1} for low-frequency and high-frequency modes, respectively. According to the conventional interpretation this means that the HF sites are more acidic than the LF sites. However, one should also emphasize that the perturbed OH stretching modes are quite broad (Maache et al.[2] reported a FWHM of 180−185 cm^{-1} of the LF mode red-shifted by 260 cm^{-1} and a width of ∼150 cm^{-1} for the HF red-shifted by 332 cm^{-1}, to be compared to a width of only about 40 cm^{-1} of the unperturbed mode), suggesting a pronounced inhomogeneity of both the HF- and LF-BA sites. Similar results are reported by Bordiga et at.[1] who failed, however, to deconvolute the HF and LF components.

1. Spectroscopy of C-Adducts. The vibrational properties of unperturbed BA sites have been discussed in section III. Calculated changes in the CO stretching frequencies due to interaction with different BA sites are listed in Tables 4 and 5. Upon interaction via the C end, the CO stretching vibrations are upshifted on average by 46 cm^{-1} (PW91), respectively and 41 cm^{-1} (RPBE), respectively, for BA sites in the main channel (i.e., Al1−O7, Al2−O2 and Al4−O10) and by 60 cm^{-1} (PW91) and 64 cm^{-1} (RPBE) for those in the small channel (i.e., Al3−O9, Al3−O6 and Al1−O6). The difference comes mainly from sites Al3−O6 and Al1−O6 in which CO is affected in addition to the attractive interaction with H atom also by repulsive interactions with framework O atoms (see Figure 11b.c and previous section).

The OH stretching frequencies of CO complexes at BA sites are collected in Table 4. For BA sites located in the main channel (i.e., Al1−O7, Al2−O2 and Al4−O10) calculated shifts of ν_{eOH} are −521 (−329) cm^{-1}, −523 (−376) cm^{-1} and −501 (−354) cm^{-1}, respectively, based on calculations with the PW91 (RPBE) functionals. Calculated $\Delta\nu_{eOH}$ for sites Al3−O9, Al3−O6 and Al1−O6 (i.e., those located in the small channel) are −617 (−466) cm^{-1}, −697 (−499) cm^{-1} and −680 (−482) cm^{-1}, respectively, i.e., on average by about 150 cm^{-1} (PW91) and 130 cm^{-1} (RPBE) larger compared to that at BA sites in the main channel.

To summarize, the results obtained using the PW91 functional, suggesting the formation of C-adducts both in the main channel and in the side-pockets, are in contradiction to experiment due to the overestimation of the shifts of both the CO and OH stretching frequencies. The results based on the RPBE functional lead to a different picture: adsorption in the side-pockets is found to be endothermic or extremely weak—hence the large shifts calculated for the CO and OH modes are irrelevant, as they will not be observed. The values of $\Delta\nu_{eCO}$ and $\Delta\nu_{eOH}$ calculated for sites in the main channel are closer to the experimentally measured values. But admittedly, to make this argument conclusive, it will be necessary to explore CO adsorption at a larger variety of BA sites. On the experimental side the question remains to be answered why N_2 is not adsorbed in the side-pockets,[5] whereas for the very similar CO molecule (molecular radius 2.149 Å for N_2, 2.238 Å for CO; no dipole moment for N_2; 0.390×10^{-30} C m for CO; polarizability 1.74 $Å^3$ for N_2, 1.95 $Å^3$ for CO; quadrupole moment -4.90×10^{-40} C m^2 for N_2, -6.73×10^{-40} C m^2 for CO) adsorption in the small channel is reported.

2. Comparison of Different Quantum Chemical Approaches. A pronounced sensitivity of the vibrational properties on the description of exchange-correlation effects is also known from cluster calculations. Deka et al.[21] used both periodic Hartree−Fock (HF) and DFT calculations (with the BLYP functional of Becke[48] and Lee, Young and Parr[49]) to study CO adsorption at clusters with three tetrahedral atoms representing a BA site. The HF calculations overestimate both the free CO and the OH stretching frequencies by about 15%. Although the calculated blue shift of the CO mode is with $\Delta\nu_{eCO} = 36$ cm^{-1} realistic, the predicted red shift of the OH-mode of $\Delta\nu_{eOH} = -77$ cm^{-1} is too small by a factor of 4. The DFT calculations using the BLYP functional produce more realistic results, $\Delta\nu_{eCO} = 48$ cm^{-1}, $\Delta\nu_{eOH} = -184$ cm^{-1}, which are closer to our value but with still significantly smaller red shifts of the OH modes. Binding energies have been reported only at the BLYP level, the value of 15.9 kJ/mol is of the same order as our RPBE values for adsorption in the main channel. Senchenya et al.[17] studied CO adsorption at Brønsted sites using a minimal dimer cluster at the HF and MP2 (Møller−Plesset perturbation theory to second order) levels. The HF results are in good agreement with those of Deka et al.; the MP2 calculations produce only a small change in the blue shift of the CO stretching mode (which is reduced from 38 to 33 cm^{-1}), but a substantially increased red shift of the OH vibrations ($\Delta\nu_{OH} = -84$ cm^{-1} (HF), −174 (MP2)), which remains, however, much smaller than that from experiment. After correction for basis-set superposition error, the calculated binding energies are ∼7 kJ/mol (HF) and ∼14 kJ/mol (MP2), the MP2 values agree roughly with our results for adsorption in the main channel. Good agreement of the calculated red shift of the OH mode is reported by Strodel et

al.[20] Their DFT calculations are based on minimal dimer clusters, self-consistency is achieved only at the LDA level, and gradient corrections using the BLYP functional are evaluated using the LDA density only. Their result of -293 cm^{-1} stands in evident contrast to the self-consistent BLYP result of Deka et al.[21] obtained for a trimer cluster. "Hybrid" functionals mix exact (HF) exchange and DFT exchange. O'Malley and Farnworth[50] presented a comparative study of CO and of weak bases (N_2, C_2H_2, C_2H_4, C_6H_6) interacting with zeolitic hydroxyl groups using dimer clusters and the BLYP and the hybrid B3LYP[51] functionals mixing 30% of exact exchange with DFT. Using the BLYP (B3LYP) functionals, the calculated harmonic frequency shifts are $\Delta\nu_{eN_2} = 12$ cm^{-1} (BLYP), 11 cm^{-1} (B3LYP) and $\Delta\nu_{eOH} = -92$ cm^{-1} (BLYP), -83 cm^{-1} (B3LYP), in reasonable agreement with the experimental results of Wakabayashi et al.,[5] $\Delta\nu_{N_2} = 5$ cm^{-1}, $\Delta\nu_{OH} = -106$ cm^{-1}. To enable a comparison, we have studied the adsorption of N_2 at the Al2$-$O2 BA site in mordenite. Our calculated harmonic frequency shifts are $\Delta\nu_{eN_2} = 11$ cm^{-1} (PW91), 5 cm^{-1} (RPBE) and $\Delta\nu_{eOH} = -262$ cm^{-1} (PW91), -108 cm^{-1} (RPBE); the RPBE results are in excellent agreement with experiment and in fair agreement with the BLYP and B3LYP results. Similar results are achieved for O_2 and H_2 adsorption; results will be reported elsewhere. The fact that the RPBE and B3LYP functionals provide a reasonable description of hydrogen bonding is also confirmed by exploratory case studies for other systems. For a methanol dimer for example, we calculate shifts of the OH-donor mode of $\Delta\nu_{eD} = -246$ cm^{-1} (PW91), -172 cm^{-1} (RPBE) and of the acceptor mode by $\Delta\nu_{eA} = 8$ cm^{-1} (PW91), 13 cm^{-1} (RPBE). Coussan et al.[52] report $\Delta\nu_{eD} = -138$ cm^{-1} and $\Delta\nu_{eA} = 6$ cm^{-1} from B3LYP calculations and $\Delta\nu_D = -140$ cm^{-1} and $\Delta\nu_A = 12$ cm^{-1} from infrared spectroscopy. Hence it appears legitimate to conclude that within DFT the RPBE functional seems to provide the most reliable description of hydrogen-bonded systems.

Farnworth and O'Malley[53] draw attention to a particular aspect of cluster calculations: depending on the orientation of terminal H_3 groups in the $H_3-Al(OH)SiH_3$ cluster, the calculated red shift of the harmonic hydroxyl mode induced by CO adsorption varies between -258 and -360 cm^{-1} in calculations using BLYP and between -233 and -297 cm^{-1} using B3LYP. We also note an evident discrepancy of their BLYP results for a dimer cluster with the BLYP results of Deka et al.[21] for a trimer cluster (cf. above). Averaged over four different rotomers of the cluster, the calculated harmonic frequency shifts are $\Delta\nu_{OH} = -305$ (-259) cm^{-1} using BLYP (B3LYP) and $\Delta\nu_{CO} = 39$ (42) cm^{-1}. The red shifts are slightly lower than our RPBE results, but given the inherent limitations of the cluster approach, it seems fair to state that RPBE and B(3)LYP perform about equally well and improve on the results obtained on the HF and MP2 level on one side, and on the PW91 level on the other side. The calculated binding energies are ~11 kJ/mol (B3LYP) and ~10 kJ/mol (BLYP), including zero-point corrections. Again, we note reasonable agreement with our RPBE results.

3. Frequency Shifts vs Adsorption Strength. Evidently, the DFT results are difficult to reconcile with the conventional interpretation of the IR spectra. Irrespective of the functional used, the DFT calculations predict a larger blue shift of the CO stretching frequencies and a larger red shift of the OH stretching modes for BA sites in the small channels than for those in the main channel. This contradicts not only the interpretation of the experimental data, it contradicts also the generally accepted correlation between adsorption strength and frequency shifts, because the weakly adsorbing BA sites in the side-pockets produce larger frequency shifts in both the adsorbate and the hydroxyl group than the strongly adsorbing sites in the main channel. This demonstrates that the frequency shifts of both the hydroxyl groups and the adsorbed molecule reflect not the strength of the interaction, but rather the electrostatic field in the vicinity of the BA site. It is evident that the field gradients are larger in the small channels than in the large ones, and this provides a natural explanation of the relative magnitude of the frequency shifts. This view is also supported by our analysis of the cluster models used to represent BA sites (see section V.A). The shift of the harmonic stretching frequency of the hydroxyl group increases systematically from -338 (-222) cm^{-1} for a one-dimensional slab model to -501 (-354) cm^{-1} for a PW91 (RPBE) calculation using the full bulk structure surrounding the BA site (see Table 2). The differences between the two GGA functionals are only quantitative: PW91 yields too large red shifts in the OH stretching frequencies that are larger by a factor of about 1.4 than using RPBE, whereas the blue shift of the CO modes remains the same within admittedly restricted statistics (although changes on individual sites can be quite large).

4. Spectroscopy of O-Adducts. Recent theoretical calculations[16,17,21] have shown that for O-adducts the CO stretching frequency is unlike that for C-adducts red-shifted, making a clear distinction between these two adsorption complexes. A frequently observed small red shift of the CO stretching frequency of about -5 cm^{-1} measured in IR experiments[1,2] is attributed to physisorbed CO, which, due to hindered rotation, forms complex structures.[55] Otero-Areán et al.[7] analyzed variable-temperature IR spectra of CO adsorbed on zeolite H$-$Y. In addition to a major band at 2173 cm^{-1} corresponding to CO adsorbed at BA sites via the C atom ($\Delta\nu_{CO} = 40$ cm^{-1}), a weak band at 2124 cm^{-1} has been detected and attributed to the OH$\cdot\cdot$OC complex ($\Delta\nu_{CO} = -19$ cm^{-1}). It has been concluded that these hydrogen-bonded species occur in the temperature-dependent equilibrium, and from the variation of their relative intensity with temperature, the difference in adsorption energies has been estimated (cf. section V.B). Our results for O-adducts are compiled in Table 5. Average shifts of CO stretching frequencies are -24 (-23) cm^{-1} and -29 (-18) cm^{-1} (calculated using the PW91 and RPBE (in parentheses) functionals) for BA sites in the main channel and in the small channel, respectively. The OH stretching frequencies of BA sites in the main channel are red-shifted by 139 (47) cm^{-1} whereas those of BA sites in the side channel are red-shifted by 213 (129) cm^{-1} on average. In agreement with recent theoretical investigations[16,17] we conclude that the existence of O-adducts cannot be excluded solely on the basis of energetics. Our calculations of the shift of the CO stretching frequency due to adsorption via the O atom agree well with IR measurements of Otero-Areán et al.[7]

The fact that C- and O-adducts differ in the sign of $\Delta\nu_{eCO}$ is remarkable: it demonstrates that the shift of the CO stretching mode is not a consequence of the adsorbate$-$substrate bonding but rather induced by the local electrostatic field close to the BA site: inversion of the direction of the dipole moment of the adsorbed CO also inverts the sign of the frequency shift. Elaborate discussion on the role of the electrostatics in the interaction of CO with various cations is given in ref 54.

VI. Terminal Silanol Groups

A. Geometry and Energetics. The interaction of CO with terminal hydroxyl groups is weaker than that with BA sites, the changes in geometry are therefore less significant. The

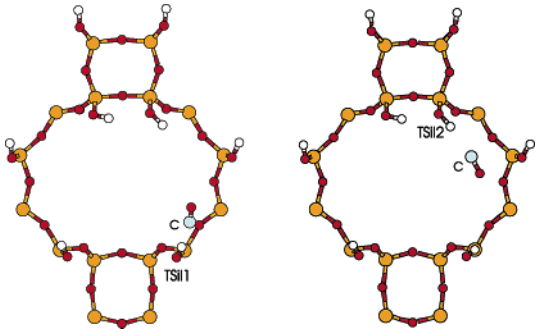

Figure 12. Carbon monoxide adsorbed at terminal silanol groups TSil1 (left) and TSil2 (right).

adsorption complexes of CO interacting through the C end with terminal silanol groups TSil1 and TSil2 are shown in Figure 12, selected structural data are collected in Tables 4 and 5. Due to weak interactions the CO bond lengths are modified only by −0.002 (−0.002) Å in C-bonded and by 0.002 (0.001) Å in O-bonded complexes, as calculated using the PW91 (RPBE) functionals. Also OH bond lengths are modified only moderately, by 0.009 (0.004) Å for C-bonded and 0.002 (−0.001) Å for O-bonded complexes. On average, as a consequence of weaker interactions, the CH distances for C-adducts and the OH distances for O-adducts are larger by about 0.2 (0.2) Å compared to those on BA sites in the main channel.

Calculated interaction energies are collected in Tables 4 and 5. For C-adducts the average binding energy is 9.6 kJ/mol in PW91 and 2.2 kJ/mol in RPBE. In the PW91 calculations, they are comparable to that for BA sites in the small channel whereas in the RPBE calculations, adsorption at the terminal silanols is exothermic, and endothermic in the side-pockets. Our results can be compared with measurements of Beebe et at.[56] who measured an isosteric heat of adsorption of 11.3 kJ/mol for terminal silanol groups of silica. The interaction energy calculated for O-adducts is about 3.1 kJ/mol (PW91) and −1.5 kJ/mol (RPBE), respectively.

B. Vibrational Properties. As already mentioned, terminal silanol groups are weak acid sites compared to bridged hydroxyl groups. This fact is reflected in smaller shifts of both the OH and CO stretching frequencies. Beebe et al.[56] found that the change in the OH stretching frequency of terminal silanol groups on a SiO_2 surface is −92 to −106 cm^{-1}, whereas $\Delta\nu_{CO}$ is 15 cm^{-1}. For USY zeolites, Daniell et al.[57] measured a downshift of ν_{OH} by −80 cm^{-1} and a blue shift of ν_{CO} by 14 cm^{-1}. Calculated CO and OH stretching frequencies for both C-adducts and O-adducts are given in Tables 4 and 5. ν_{eCO} for CO bound via the C end is increased by 24 and 26 cm^{-1} (PW91) and 16 and 28 cm^{-1} (RPBE). ν_{eOH} decreases by 178 and 192 cm^{-1} (PW91) and by 99 and 107 cm^{-1} (RPBE) for sites TSil1 and TSil2, respectively. Although the choice of the exchange-correlation functional is for terminal silanols not as dramatic as for BA sites, the RPBE results are definitely in better agreement with experiment.

As for BA sites, the CO stretching frequencies for O-adducts at terminal silanols are red-shifted, the calculated $\Delta\nu_{eCO}$ is −16 and −18 cm^{-1} (PW91) and −2 and −12 cm^{-1} (RPBE) for sites TSil1 and TSil2, respectively. Changes in the OH stretching frequencies are only −28 and −52 cm^{-1} for sites TSil1 and TSil2, respectively. Surprisingly, the RPBE calculations predict even a blue shift of the OH stretching frequencies by 17 and 6 cm^{-1}, respectively. Although small red shifts of CO stretching frequency by about 9 cm^{-1} at high coverages of CO at SiO_2 surfaces were reported experimentally,[56] this effect was assigned to a solvent effect where the CO species adsorbed at silanol groups play the role of the solute and where several layers of CO molecules that do not interact directly with OH groups play the role of the solvent.[56]

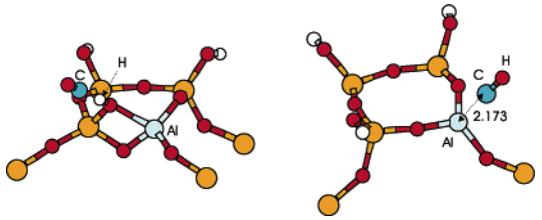

Figure 13. Detailed view of adsorption complexes of CO at defect with BA site at two-membered ring (left) and at defect with 3-fold coordinated Al site.

VII. Surface Defects

In Figure 5a a defect with a strained two-membered ring (2MR) which represents a weak Lewis site is shown. Neither of the possible interaction centers (Si or O atoms of the 2MR) forms a stable adsorption complex with a CO molecule. Irrespective of the orientation of the CO molecule relative to the 2MR in the starting configuration, in the relaxed structure the shortest distance between the CO molecule and the 2MR is larger than 3 Å, the CO bond as well as the geometry of the defect are essentially unaffected by interaction. Binding energies for all tested configurations are smaller than 2 kJ/mol using both PW91 and RPBE functionals.

A defect with a BA site at a two-membered ring (2MR−Al) (Figure 5b) is a weak BA site. The calculated OH stretching frequency (3780 cm^{-1} using PW91 and 3773 cm^{-1} using RPBE functional, respectively) is about halfway between BA sites and isolated terminal silanol groups (see Table 1). The adsorption complex with a C-adduct at the 2MR−Al is shown in Figure 13, selected structural data are compiled in Table 4. The intermolecular separation between CO and H atom of 2MR−Al is 1.989 (2.105) Å using the PW91 (RPBE) functionals, i.e., by about 0.080 (0.061) Å larger compared to the average value calculated for BA sites in the main channel and by about 0.153 (0.179) Å smaller compared to adsorption at terminal OH groups. The CO bond length is shortened by 0.004 (0.005) Å, and the OH bond is elongated by 0.014 (0.009) Å compared to unperturbed CO and 2MR−Al, respectively. These changes in geometry are accompanied by a blue shift of the CO stretching vibration by 38 (40) cm^{-1}, and by a red shift of the OH stretching vibration by 322 (231) cm^{-1}. The binding energy for this adduct is 15.4 (8.3) kJ/mol, i.e., higher by only 5.8 (6.1) kJ/mol than for terminal silanol groups. All these results show that the acidity of the 2MR−Al defect site is mid-way between BA and TSil sites. For an O-adduct, the CO stretching frequency is red-shifted by 21 (15) cm^{-1}, and the OH stretching frequency is red-shifted by 74 (26) cm^{-1}. The separation between CO and the H atom of the defect is 1.992 (2.159) Å. The changes in the CO bond length (0.002 Å in PW91 and 0.001 in RPBE calculations) and in the length of the HO_Z group (0.003 Å (PW91) and 0.001 (RPBE)) are similar to the corresponding parameters for O-adducts at terminal silanol groups. The calculated binding energy is 5.5 kJ/mol using PW91 and 1.3 kJ/mol using RPBE functionals, respectively.

A defect with a 3-fold coordinated Al atom (3-Al) shown in Figure 5c represents a strong Lewis site. The calculated blue shift of the CO stretching frequency for the C-adduct, displayed in Figure 13 is 62 cm^{-1} using PW91 and 65 cm^{-1} using RPBE functionals, respectively (see Table 4). Taking this quantity as

a measure of acidity, the defect with a 3-fold coordinated Al atom belongs to the most acidic sites investigated in this study (see Table 4). The change in the CO bond length is −0.008 (−0.008) Å, the C−Al separation is 2.173 (2.230) Å. The interaction of carbon monoxide with 3-fold coordinated Al site is by about 25 kJ/mol stronger than the strongest interactions with BA sites, the calculated binding energy is 52.1 (32.6) kJ/mol using PW91 (RPBE) functionals. Upon adsorption of CO through the O end, the CO bond is elongated by 0.003 (0.003) Å, and the CO stretching frequency is decreased by 37 (33) cm^{-1}. The binding energy for this complex is 16.9 (2.1 kJ/mol. Although 3-fold coordinated framework Al sites have been evidenced recently by X-ray absorption spectroscopy at the Al K-edge,[58] experimental data on adsorption of CO on such a defect are not available. Generally, in the IR spectra strong Lewis sites are evidenced by the presence of a band above 2190 cm^{-1}, i.e., by a blue shift of the CO stretching frequency by more than 50 cm^{-1},[47] in good agreement with our present results.

VIII. Discussion and Conclusion

Evidently, the results of our DFT study of the adsorption and the vibrational spectroscopy of CO in mordenite challenge some of notions on the vibrational spectroscopy of small probe molecules adsorbed in zeolites. Because the gradient-corrected PW91 exchange-correlation functional was found to overestimate the strength of hydrogen bonding between the probe molecule and the bridging OH groups, the RPBE functional was explored as an alternative. In comparing with the PW91 results we find a strongly reduced adsorption energy and much smaller red shift of the OH stretching frequencies. To support the argument that the RPBE functional results in a more realistic description of hydrogen bonding, the comparison of the PW91 and RPBE functionals was extended to other probe molecules adsorbed at Brønsted acid sites and to hydrogen-bonded molecular dimers.

Returning to CO in mordenite, we find that for terminal silanol groups and for tricoordinated Al atoms (i.e., for very weak BA sites and for a strong Lewis site) our predictions based on the RPBE functional agree reasonably well with the experimental estimates of adsorption energy and frequency shifts. For the adsorption at bridging OH groups, however, our results disagree with two fundamental assumptions underlying the interpretation of the measured IR spectra: (i) Stronger adsorption (i.e., larger adsorption energy) parallels a stronger red shift of the OH mode and a stronger blue shift of the CO mode. (ii) CO molecules adsorbed in the main channel induce a stronger red shift of the OH modes than molecules adsorbed in the side-pocket. In contrast, we calculate using both functionals much larger red shifts for adsorption in the small channels—too large to be compatible with experiment even with the RPBE functional. However, this functional predicts vanishing or even endothermic adsorption energies for CO in the side-pockets, so that the large red shifts should indeed not be observable. From microcalorimetry measurements[10] it was concluded that all BA sites in mordenite are energetically equivalent; evidently, this supports our result that only sites in the main channel are accessible to CO molecules. We also note that the measured difference for adsorption in the purely siliceous zeolite and at BA sites agrees very well with our RPBE result and that the remaining difference between the RPBE energies and experiment is reasonably well accounted for by van der Waals forces.

We discuss first the correlation between adsorption strength and frequency shifts. The conventional physical picture of bond formation on CO adsorption is based on the concept of donation and back-donation: donation of electrons from the occupied 5σ molecular orbitals of CO to form an adsorbate−substrate bond, and back-donation from the substrate to the empty $2\pi^*$ orbitals (see, e.g., the work of Strodel et al.[20]). The former effect depletes the bonding orbitals of the molecule, whereas the latter fills the antibonding states. Hence both donation and back-donation weaken the intramolecular bond and can explain only a red shift of the stretching mode. The fact that adsorption at a BA site in a zeolite induces a blue shift indicates a different bonding mechanism. The hydrogen bond between a BA site and the C atom of the molecule is essentially of electrostatic character. The preference for the formation of a C-adduct corresponds to the sign of the small dipole moment of CO. Bond formation is enhanced by the polarizability of the molecule and the hydroxyl group. In addition, the electrostatic field created by the charged zeolitic framework is important. This electrostatic field modifies the potential energy surface of both the hydroxyl group and the CO molecule and is of prime importance in determining the frequency shifts. The gradients of the electrostatic field are necessarily stronger in the small channels—this explains the surprising fact that larger shifts of both the CO and the OH stretching modes in the small channels correlate with lower adsorption energies.

The other point where theory and interpretation of experiments diverge concerns the predicted inaccessibility of the side-pockets for CO molecules. Although Wakabayashi et al.[5] concluded that the side-pockets in mordenite are inaccessible to N_2, O_2 and H_2 molecules, and Cairon et al.[6] reported that the sodalite cages in zeolite Y do not admit CO molecules, the interpretation of the IR spectra of CO adsorbed in mordenite is still based on the assumption of adsorption in both the main channel and in the side-pocket. This assumption is based on the asymmetry of the OH and CO bands in the IR spectra, which may be deconvoluted into HF and LF components. It must be emphasized, however, that the widths of both components are by far larger than their separation and that microcalorimetry suggests all BA sites accessible to CO to be energetically homogeneous.[10]

Ab initio calculations using periodic models of zeolites provide the first opportunity to test some of these assumptions. In the previous work by Demuth et al.[31] seven different acid sites in the main channel of mordenite have been considered—their OH stretching frequencies span a range of 58 cm^{-1}, to be compared with a difference of ∼27 cm^{-1} between the centers of the HF and LF modes derived from the fitted IR spectra. In the present work we have considered three BA sites in the main channel (spanning a range of 51 cm^{-1}) and three BA sites in the side-pockets (distributed over 21 cm^{-1}), the difference in the average OH stretching frequencies being only 8 cm^{-1} (calculations using RPBE, PW91 produces a slightly narrower distribution and a slightly lower difference). Admittedly, this does not allow us to establish a good statistics, but it is evident that the frequency distributions of hydroxyl groups in the main channel and in the side-pocket largely overlap, indicating a pronounced inhomogeneity of both types of BA sites.

To the best of our knowledge, our work is also the first to study CO adsorption in a periodic model of a complex zeolite, all previous investigations are based on cluster models and hence cannot distinguish between adsorption in large and small cavities. Our prediction that CO adsorption in the side-pockets is energetically disfavored must be seen in relation to studies involving other probe molecules. As already mentioned above, the small channels are inaccessible to homonuclear dimers,

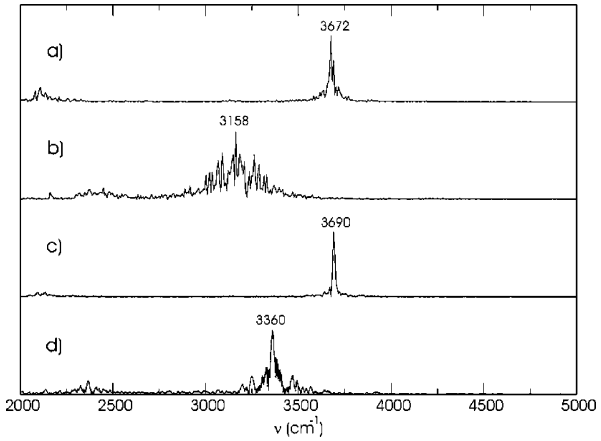

Figure 14. Molecular dynamics simulations at $T = 100$ K, FFT of the velocity autocorrelation function calculated for (a) unperturbed zeolite with acid site in position Al2−O2, calculated using the PW91 functional; (b) OH group modified by the CO adsorption, PW91 calculation; (c) and (d) as (a) and (b), respectively, but calculated using the RPBE functional.

whereas the bulkier and more basic ammonia molecule is adsorbed even more strongly in the side-pockets than in the main channel.[41] The reason is that ammonia is protonated by BA sites and forms multiple bonds with framework oxygens in a favorable adsorption geometry. Given its weak basicity, the chemistry of CO adsorption will be closer to that of the homonuclear dimers.

We cannot at the moment offer an explanation for the fact that preadsorption of a large, basic molecule such as pyridine blocks certain BA sites in the main channel whereas others remain accessible to CO.[2] This must be left to future investigations. Also, the adsorption of CO in the presence of preadsorbed pyridine deserves a critical examination. Pyridine will certainly by protonated by the strong BA sites in the main channel and the related charge redistribution is likely to influence the hydrogen bonding of coadsorbates.

All results presented in our paper are based on the harmonic approximation. The corrections for anharmonicity can modify the frequency shifts for the OH stretching mode induced by the adsorption of a CO molecule. We have made some preliminary investigations to appreciate the role of the anharmonicity on the vibrational properties of adsorption complexes. For this purpose we used two different methods:

1. Solving the One-Dimensional Schrödinger Equation for the Potential along the OH Stretching Vibrational Mode (Program ANHARM by P. Ugliengo[59]). The potential energies have been calculated for thirteen different structures with the OH group deformed in the interval from −0.20 to +0.28 Å and the potential has been approximated by a sixth-degree polynomial. The anharmonicity parameter $2\nu_e\chi_e$ has been calculated from the difference in the frequencies of two lowest vibrational states ν_{01} and ν_{02} using the formula $2\nu_e\chi_e = \nu_{02} - \nu_{01}$.

2. An Initio Molecular Dynamics. The anharmonic frequencies are determined from the Fourier transform of the velocity autocorrelation function. Molecular dynamics simulations have been performed at $T = 100$ K, simulation time was 5 ps.

Some of our preliminary results for the Brønsted acid site Al2−O2 are shown in Figure 14 and Table 6. The two approaches provide distinctly different results—whereas the MD approach leads to temperature dependent shifts of the OH stretching frequency, which are at low temperatures remarkably similar to those calculated on the basis of harmonic approximation, the OH shifts obtained by solving the one-dimensional Schrödinger equation are increased by ∼25% compared to the harmonic approximation results. We note that in the current literature only the first method is used.[17,60−63] Our results suggest that estimates of anharmonicity based on a purely one-dimensional approach are of limited validity. Furthermore our MD studies emphasize that anharmonic frequency shifts are necessarily temperature dependent. At a temperature of $T = 100$ K (corresponding to the temperature at which the IR spectra are usually measured), the frequencies derived from the MD simulations are still rather close to the harmonic values. We are currently extending the very time-consuming MD simulations. As to our knowledge no experimental data are avaliable on how the anharmonicity of OH stretching mode is modified upon adsorption of CO, we leave this problem for further, more detailed study.

TABLE 6: Vibrational Frequencies (cm^{-1}) for the OH Group of the Brønsted Acid Site Al2−O2 in the Unperturbed Mordenite and in the Adsorption Complex with Carbon Monoxide Calculated Using the Molecular Dynamics, Solving the One-Dimensional Schrödinger Equation and Using the Harmonic Approximation

	molecular dynamics		one-dim. Schrödinger eq.		harmonic approximation	
	unpert.	OH···CO	unpert.	OH···CO	unpert.	OH···CO
PW91	3672	3158	3579	2933	3728	3205
RPBE	3690	3360	3589	3111	3742	3366

[a] The PW91 and RPBE results are listed.

Hence although periodic DFT studies are far from resolving all questions, they certainly shed a new light on the molecular adsorption in zeolites and on their chemical reactivity.

Acknowledgment. This work has been performed with the Science College "Computational Materials Science", supported by the Austrian Science Funds. L.B. acknowledges financial support from the Institut Francais du Pétrole within the Groupement de Recherche Européen (GdR-E) "Dynamique moléculaire quantique appliquée à la catalyse". Facilities at Computing Center of Vienna University (Schrödinger cluster) are kindly acknowledged.

References and Notes

(1) Bordiga, S.; Lamberti, C.; Geobaldo, F.; Zecchina, A.; Turnes Palomino, G.; Zecchina, A. *Langmuir* **1995**, *11*, 527.
(2) Maache, M.; Janin, A.; Lavalley, J. C.; Benazzi, E. *Zeolites* **1995**, *15*, 507.
(3) Webster, Ch. E.; Cottone, A.; Drago, R. S. *J. Am. Chem. Soc.* **1999**, *121*, 12127.
(4) Zholobenko, V. L.; Makarova, M. A.; Dwyer, J. *J. Phys. Chem.* **1993**, *97*, 5962.
(5) Wakabayashi, F.; Kondo, J. N.; Wada, A.; Domen, K.; Hirose, C. *J. Phys. Chem.* **1993**, *97*, 10761.
(6) Cairon, O.; Chevreau, T. *J. Chem. Soc., Faraday Trans.* **1998**, *94*, 323.
(7) Otero-Areán, C.; Tsyganenko, A. A.; Manoilova, O. V.; Palomino, G. T.; Mentruit, M. P.; Garrone, E. *Chem. Commun.* **2001**, 455.
(8) Bordiga, S.; Turnes Palomino, G.; Pazè, C.; Zecchina, A. *Microporous Mesoporous Mater.* **2000**, *34*, 67.
(9) Wakabayashi, F.; Fujino, T.; Kondo, J. N.; Domen, K.; Hirose, C. *J. Phys. Chem.* **1995**, *99*, 14805.
(10) Savitz, S.; Myers, A. L.; Gorte, R. J. *J. Phys. Chem. B* **1999**, *103*, 3687.
(11) Bolis, V.; Broyer, M.; Barbaglia, A.; Busco, C.; Foddanu, G. M.; Ugliengo, P. *J. Mol. Catal. A* **2003**, *204−205*, 561.
(12) Catana, G.; Baetens, D.; Mommaerts, T.; Schoonheydt, R. A.; Weckhuysen, B. M. *J. Phys. Chem. B* **2001**, *105*, 4904.
(13) Kustov, L. M.; Kazansky, V. B.; Beran, S.; Kubelková, L.; Jiru, P. *J. Phys. Chem.* **1987**, *91*, 5247.
(14) Gruver, V.; Fripiat, J. J. *J. Phys. Chem.* **1994**, *98*, 8549.
(15) Gruver, V.; Panov, A.; Fripiat, J. J. *Langmuir* **1996**, *12*, 2505.

(16) Sauer, J.; Ugliengo, P.; Garrone, E.; Saunders, V. R. *Chem. Rev.* **1994**, *94*, 2095.
(17) Senchenya, I. N.; Garrone, E.; Ugliengo, P. *J. Mol. Struct. (THEOCHEM)* **1996**, *368*, 93.
(18) Bates, S.; Dwyer, J. *J. Phys. Chem.* **1993**, *97*, 5897.
(19) Neyman, K. M.; Strodel, P.; Ruzankin, S. P.; Schlensog, W.; Knözinger, H.; Rösch, N. *Catal. Lett.* **1995**, *31*, 273.
(20) Strodel, P.; Neyman, K. M.; Knözinger, H.; Rösch, N. *Chem. Phys. Lett.* **1995**, *240*, 547.
(21) Deka, R. C.; Tajima, N.; Hirao, K. *J. Mol. Struct. (THEOCHEM)* **2001**, *535*, 31.
(22) Limtrakul, J.; Khongpracha, P.; Jungsuttiwong, S.; Truong, T. N. *J. Mol. Catal. A* **2000**, *153*, 155.
(23) Limtrakul, J.; Jungsuttiwong, S.; Khongpracha, P. *J. Mol. Struct.* **2000**, *525*, 153.
(24) Wesołowski, T. A.; Goursot, A.; Weber, J. *J. Chem. Phys.* **2001**, *115*, 4791.
(25) Kresse, G.; Hafner, J. *Phys. Rev. B* **1993**, *48*, 13115.
(26) Kresse, G.; Hafner, J. *Phys. Rev. B* **1994**, *49*, 14251.
(27) Kresse, G.; Furthmüller, J. *Comput. Mater. Sci.* **1996**, *6*, 15.
(28) Kresse, G.; Furthmüller, J. *Phys. Rev. B* **1996**, *54*, 11196.
(29) Perdew, J. P.; Chewary, J. A.; Vosko, S. H.; Jackson, K. A.; Pedersen, M. R.; Singh, D. J.; Fiolhais, C. *Phys. Rev. B* **1992**, *46*, 6671.
(30) Perdew, J. P.; Wang, Y. *Phys. Rev. B* **1992**, *45*, 13244.
(31) Demuth, T.; Hafner, J.; Benco, L.; Toulhoat, H. *J. Phys. Chem. B* **2000**, *104*, 4593.
(32) Jeanvoine, Y.; Angyan, J. G.; Kresse, G.; Hafner, J. *J. Phys. Chem. B* **1998**, *102*, 573.
(33) Benco, L.; Demuth, T.; Hafner, J. *J. Chem. Phys.* **1999**, *111*, 7537.
(34) Gajdos, M.; Eichler, A.; Hafner, J. *J. Phys. Condens. Mater.* **2004**, *16*, 1141.
(35) Perdew, J. P.; Burke, K.; Ernzerhof, M. *Phys. Rev. Lett.* **1996**, *77*, 3865.
(36) Hammer, B.; Hansen, L. B.; Nørskov, J. K. *Phys. Rev. B* **1999**, *59*, 7413.
(37) Blöchl, P. E. *Phys. Rev. B* **1994**, *50*, 17953.
(38) Kresse, G.; Joubert, D. *Phys. Rev. B* **1999**, *59*, 1758.
(39) Bucko, T.; Benco, L.; Demuth, Th.; Hafner, J. *J. Chem. Phys.* **2002**, *117*, 7295.
(40) Ángyán, J. G.; Parsons, D.; Jeanvoine, Y. *Ab initio simulations of zeolites reactivity* in *Theoretical aspects of heterogeneous catalysis*; Chaer Nascimento, M. A., Ed.; Kluwer Academic Publishers: Dordrecht, The Netherlands, 2001; pp 77−108.
(41) Bucko, T.; Hafner, J.; Benco, L. *J. Chem. Phys.* **2004**, *120*, 10263.
(42) Schlenker, J. L.; Pluth, J. J.; Smith, J. V. *Mater. Res. Bull.* **1979**, *14*, 751.
(43) Bucko, T.; Benco, L.; Hafner, J. *J. Chem. Phys.* **2003**, *118*, 8437.
(44) Huber, K. P.; Herzberg, G. *Molecular Spectra and Molecular Structure Constants of Diatomic Molecules*; van Nostrand-Reinhold: New York, 1979.
(45) Hehre, W. J.; Radom, L.; Schleyer, P. v. R.; Pople, J. A. *Ab Initio Molecular Orbital Theory*; Wiley: New York, 1986.
(46) Breck, D. W. *Zeolite Molecular Sieves*; Wiley-Interscience: New York, 1974; p 460.
(47) Lercher, J. A.; Gründling, Ch.; Eder-Mirth, G. *Catal. Today* **1996** *27*, 353.
(48) Becke, A. D. *Phys. Rev. A* **1988**, *38*, 3098.
(49) Lee, C.; Yang, W.; Parr, R. G. *Phys. Rev. B* **1988**, *37*, 785.
(50) O'Malley, P. J.; Farnworth, K. J. *J. Phys. Chem. B* **1998**, *102*, 1814.
(51) Stephens, P. J.; Devlin, J. F.; Chabalowski, C. F.; Frisch, M. J. *J. Phys. Chem.* **1994**, *98*, 11623.
(52) Coussan, S.; Bouteiller, Y.; Loutellier, A.; Perchard, J. P.; Racine, S.; Peremans, A.; Zheng, W. Q.; Tadjeddine, A. *Chem. Phys.* **1997**, *219*, 221.
(53) Farnworth, K. J.; O'Malley, P. J. *J. Phys. Chem.* **1996**, *100*, 1814.
(54) Ferrari, A. M.; Ugliengo, P.; Garrone, E. *J. Chem. Phys.* **1996**, *105*, 4129.
(55) Ewing, G. E. *J. Chem. Phys.* **1962**, *37*, 2250.
(56) Beebe, T. P.; Gelin, P.; Yates, J. T. *Surf. Sci.* **1984**, *148*, 526.
(57) Daniell, W.; Topsøe, N. Y.; Knözinger, H. *Langmuir* **2001**, *17*, 6233.
(58) van Bokhoven, J. A.; van der Eerden, A. M. J.; Koningsberg, D. C. *J. Am. Chem. Soc.* **2003**, *125*, 7435.
(59) Ugliengo, P.; ANHARM − A program to solve monodimensional nuclear Schrødinger equation, 1989, unpublished.
(60) Civalleri, B.; Garrone, E.; Ugliengo, P. *J. Mol. Struct. (THEOCHEM)* **1997**, *419*, 227.
(61) Senchenya, I. N.; Civalleri, B.; Ugliengo, P.; Garrone, E. *Surf. Sci.* **1998**, *412/413*, 141.
(62) Ugliengo, P.; Civalleri, B.; Dovesi, R.; Zicovich-Wilson, C. M. *Phys. Chem. Chem. Phys.* **1998**, *1*, 545.
(63) Mérawa, M.; Civalleri, B.; Ugliengo, P.; Noël Y.; Lichanot, A. *J. Chem. Phys.* **2003**, *1*, 1045.